Am J Physiol Regul Integr Comp Physiol 291: R1781–R1789, 2006.
First published August 3, 2006; doi:10.1152/ajpregu.00421.2006.

Calcium flux in turtle ventricular myocytes

Gina L. J. Galli,[1,2] Edwin W. Taylor,[2] and Holly A. Shiels[1]

[1]*Faculty of Life Sciences, The University of Manchester, Core Technology Facility, Manchester, United Kingdom; and* [2]*School of Biosciences, The University of Birmingham, Birmingham, United Kingdom*

Submitted 15 June 2006; accepted in final form 2 August 2006

Galli, Gina L. J., Edwin W. Taylor, and Holly A. Shiels. Calcium flux in turtle ventricular myocytes. *Am J Physiol Regul Integr Comp Physiol* 291: R1781–R1789, 2006. First published August 3, 2006; doi:10.1152/ajpregu.00421.2006.—The relative contribution of the sarcoplasmic reticulum (SR), the L-type Ca^{2+} channel and the Na^+/Ca^{2+} exchanger (NCX) were assessed in turtle ventricular myocytes using epifluorescent microscopy and electrophysiology. Confocal microscopy images of turtle myocytes revealed spindle-shaped cells, which lacked T-tubules and had a large surface area-to-volume ratio. Myocytes loaded with the fluorescent Ca^{2+}-sensitive dye Fura-2 elicited Ca^{2+} transients, which were insensitive to ryanodine and thapsigargin, indicating the SR plays a small role in the regulation of contraction and relaxation in the turtle ventricle. Sarcolemmal Ca^{2+} currents were measured using the perforated-patch voltage-clamp technique. Depolarizing voltage steps to 0 mV elicited an inward current that could be blocked by nifedipine, indicating the presence of Ca^{2+} currents originating from L-type Ca^{2+} channels (I_{Ca}). The density of I_{Ca} was 3.2 ± 0.5 pA/pF, which led to an overall total Ca^{2+} influx of 64.1 ± 9.3 μM/l. NCX activity was measured as the Ni^+-sensitive current at two concentrations of intracellular Na^+ (7 and 14 mM). Total Ca^{2+} influx through the NCX during depolarizing voltage steps to 0 mV was 58.5 ± 7.7 μmol/l and 26.7 ± 3.2 μmol/l at 14 and 7 mM intracellular Na^+, respectively. In the absence of the SR and L-type Ca^{2+} channels, the NCX is able to support myocyte contraction independently. Our results indicate turtle ventricular myocytes are primed for sarcolemmal Ca^{2+} transport, and most of the Ca^{2+} used for contraction originates from the L-type Ca^{2+} channel.

reptile; excitation-contraction coupling; sarcoplasmic reticulum; Na^+/Ca^{2+} exchanger; L-type Ca^{2+} channel

FROM THE SIMPLE TWO-CHAMBERED heart of fish to the completely divided four-chambered heart of mammals, the structure and function of the vertebrate heart are remarkably varied. Nevertheless, the basic cellular process that underpins the cardiac contraction and relaxation cycle is common to all vertebrate hearts. This process, termed "excitation-contraction coupling" (E-C coupling), begins with excitation of the myocyte membrane, leads to a rise in intracellular Ca^{2+}, and culminates in activation and contraction of the myofilaments. Both the rate and magnitude of myofilament contraction depends on the rise and fall of intracellular Ca^{2+}, and thus cellular cycling of Ca^{2+} forms the basis of E-C coupling. There are two main ways Ca^{2+} can be delivered and removed from the myocyte: *1*) Ca^{2+} can be cycled across the sarcolemmal membrane via L-type Ca^{2+} channels or the Na/Ca^{2+} exchanger (NCX) and *2*) Ca^{2+} can be cycled within the myocyte from intracellular stores of Ca^{2+}, such as the sarcoplasmic reticulum (SR) (6). However, although the process of E-C coupling is common to all vertebrate hearts, there are important interspecific differences in the way Ca^{2+} is cycled to and from the myofilaments.

SR and sarcolemmal Ca^{2+} cycling can vary between species (3, 6, 16, 21, 32, 33, 36), different stages of development (14, 27, 28), and regionally within the heart (6, 25). In most fish and amphibians, transsarcolemmal Ca^{2+} influx is the primary source of activator Ca^{2+} responsible for initiating contraction (1, 26, 31, 39, 44). The majority of this extracellular Ca^{2+} enters the cell through L-type Ca^{2+} channels, although in some species, the NCX may also contribute significant amounts of activator Ca^{2+} (19, 34, 42). The contribution of intracellular Ca^{2+} cycling through the sarcoplasmic reticulum (SR) is minimal in most ectothermic vertebrates and varies subject to experimental conditions (6, 12, 13, 21, 31). In contrast, activation of the myofilaments in most adult mammalian hearts occurs mainly through the mobilization of the intracellular Ca^{2+} stores of the SR, with sarcolemmal Ca^{2+} influx primarily acting as a trigger for SR Ca^{2+} release (6).

The regulation of contraction with respect to Ca^{2+} cycling has never been studied on a cellular level in any reptilian species. Recently, we have shown isolated turtle ventricular muscle to be relatively insensitive to ryanodine, a compound that inhibits the SR Ca^{2+} release channel. These results suggest that, similar to fish, the SR contributes little Ca^{2+} to turtle heart contraction and relaxation (12). In the absence of a functional SR, we would hypothesize that sarcolemmal Ca^{2+} transport is the primary source of Ca^{2+} and that the NCX is the primary Ca^{2+} efflux pathway. The aim of the present study was to confirm this hypothesis experimentally. Here, we have examined the contribution of the cardiac L-type Ca^{2+} channel, the NCX, and the SR to contraction and relaxation in single isolated ventricular myocytes from the turtle heart. Our results confirm our hypothesis that transsarcolemmal flux is the primary route for Ca^{2+} transport in turtle ventricular myocytes. Moreover, our data provide the groundwork for future studies on ion regulation of contractility in reptilian cardiomyocytes.

MATERIALS AND METHODS

Animal Origin and Care

Yellow-bellied turtles, *Trachemys scripta scripta* (body mass = 218.5 ± 23.9 g, heart mass = 0.61 ± 0.1 g, n = 12) were obtained from Monkfield Nutrition Ltd (Hertfordshire, UK). Turtles were held in 1.5 × 0.5 × 0.5 m plastic tanks containing water maintained at 20–21°C (40 cm depth) and dry basking platforms, allowing access to heating lamps for behavioral thermoregulation.

Address for reprint requests and other correspondence: G. L. J. Galli, Faculty of Life Sciemces, The Univ. of Manchester, Core Technology Facility, 46 Grafton St., Manchester, M13 9NT UK (e-mail: ginaljgalli@hotmail.com).

The costs of publication of this article were defrayed in part by the payment of page charges. The article must therefore be hereby marked "*advertisement*" in accordance with 18 U.S.C. Section 1734 solely to indicate this fact.

Table 1. *Morphometric measurements of turtle ventricular myocytes*

Cell length, μm	Cell width, μm	Cell depth, μm	Cell capacitance, pF	Cell volume, pl	Ratio, pF/pl
189.1 ± 10.3	7.2±0.4	5.4±0.3	42.4±1.9	2.3±0.1	18.3

Data are expressed as means ± SE, $n = 18$. Cell length, width, and depth were measured by analysis of confocal microscopy images of myocytes. Cell volume was derived from cell capacitance.

Solutions

The isolation solution contained (in mM) 100 NaCl, 10 KCl, 1.2 KH_2PO_4, 4 $MgSO_4$, 50 taurine, 20 glucose, and 10 HEPES, with pH adjusted to 6.9 via KOH. For enzymatic digestion, 1.5 mg/ml collagenase (type 1A), 1 mg/ml trypsin (type IX), and 1.5 mg/ml fatty acid-free BSA were added to the solution. The extracellular solution perfusing the myocytes contained (in mM) 150 NaCl, 5.4 CsCl, 1.5 $MgSO_4$, 0.4 NaH_2PO_4, 2 $CaCl_2$, 10 glucose, 10 HEPES, with pH adjusted to 7.7 via CsOH. For whole cell voltage-clamp electrophysiological measurements, the pipette solution contained (in mM) 130 CsCl, 1 $MgCl_2$, 5 MgATP, 5 Na_2-phosphocreatine (unless stated otherwise), 10 HEPES, 15 tetraethylammonium chloride (TEA), and 0.03 Na_2GTP. The EGTA concentration was 0.025 mM unless stated otherwise. The pH was adjusted to 7.2 with CsOH. Including TEA and CsOH abolished all K^+ currents. In perforated-patch, voltage-clamp experiments, 240 μg/ml amphoteracin was added to the pipette solution. To be certain that cells were indeed perforated and not in the whole cell configuration, a high concentration of $CaCl_2$ (10 mM) was also included in the pipette solution. All drugs were purchased from Sigma Aldrich.

Isolated Myocyte Preparation

Myocytes were obtained by adaptation of isolation protocols previously described for fish (32, 34, 42). All procedures were made in accordance with UK Home Office regulations. Briefly, turtles were euthanized by decapitation, and the head was immediately submerged into liquid nitrogen to fully destroy all neural connections. A 2 cm × 2 cm piece of the ventral plastron was removed above the heart using a bone saw. The heart was excised and a cannula was inserted into the right aortic arch and advanced into the ventricle for perfusion. The heart was retrogradely perfused for 10 min at room temperature first with isolation solution to clear the heart of blood and to stop the heart contracting and then with proteolytic enzymes (BSA, collagenase, and trypsin) for a further 20 min. The enzyme solution was retained for use later. Ventricular tissue was separated from the atria, cut into small pieces with scissors, and placed in the collected enzyme solution and shaken at 34°C (Grant OLS200 water bath shaker). To check for viable myocytes, aliquots of tissue suspension were taken every 5 min and placed under a microscope. Once viable myocytes were observed, the suspension was removed from the shaker, left to settle, and resuspended in fresh isolation solution. Healthy viable cells were usually obtained after 15–20 min of heating and shaking. Myocytes were agitated gently, filtered through a nylon mesh, and stored in fresh isolation solution at room temperature for up to 8 h.

Myocyte Morphometrics

To obtain measurements of myocyte dimensions, cells were imaged using confocal microscopy. The sarcolemmal membrane of the myocytes were visualized by loading cells for 10 min with the lipophilic fluorescent indicator di-8-ANNEPS (5 μM, Molecular Probes). Cells were then resuspended in fresh isolation solution and imaged using a laser scanning confocal microscope (Leica, Germany) with 488-nm excitation light and detection at >505 nm. Consecutive plane scans (*x-y*) were made through the cell to make a three-dimensional model (*z* stack), from which cell length, width, depth, and volume were calculated using the Zeiss LSM image browser 5.0 software program (see Table 1).

Fluorescent Measurements of $[Ca^{2+}]_i$ Using Fura-2 AM

To record changes in $[Ca^{2+}]_i$, ventricular myocytes were loaded with the AM form of the Ca^{2+}-sensitive fluorescent dye Fura-2 (Molecular Probes) to a final concentration of 4 μmol/l. Myocytes were shaken gently for 10 min to allow loading; then a sample of the cells were placed on the stage and left to settle for a further 5 min. Cells were then perfused for 15–20 min with extracellular solution for deesterification. All fluorescent measurements were conducted at room temperature. To examine the contribution of the SR to Ca^{2+} flux in turtle myocytes, cells were field stimulated to contract at 0.2 and 0.5 Hz in the presence and absence of SR blockade [10 μmol/l ryanodine and 2 μmol/l thapsigargin (Sigma Aldrich)]. To ensure complete inhibition of the SR, cells were perfused with ryanodine and thapsigargin for a period of 5 min before measurements were commenced. The ratio of the fluorescence emitted at 510 nm in response to alternate illumination with light at 340 and 380 nm (Cairn Research) was used as our index of $[Ca^{2+}]_i$.

Electrophysiological Measurements of Sarcolemmal Currents

Samples of myocytes were added to the recording chamber and left to settle and attach to the bottom. Cells were perfused with extracellular solution at a rate of 1–2 ml/min at room temperature (~21°C). Both whole cell and perforated-patch, voltage-clamp experiments were performed using an Axopatch 200B amplifier (Axon Instruments) with a CV 203BU headstage (Axon Instruments). Patch pipettes were pulled with borosilicate glass (Harvard Apparatus) and had a resistance of 2.4 ± 0.02 MΩ when filled with pipette solution. In perforated-patch, voltage-clamp experiments, once a gigaohm seal had formed, patch pipette resistance (5–6 MΩ) was compensated for, and Ra was monitored using the membrane test function to assess the extent of perforation. Once electrical access to the cell was gained, the cell capacitive currents were compensated for by manually adjusting series resistance (Ra) and the cell capacitance compensation circuits. Series resistance [whole cell Ra = 8.2 ± 0.9 MΩ ($n = 38$); perforated Ra = 17.2 ± 1.5 MΩ ($n = 40$)] and capacitance [Cm = 42.4 ± 1.9 pF ($n = 78$)] were measured using the membrane test function of pClamp 9.0 software (Axon Instruments). In the perforated-patch configuration, Ra was monitored throughout the experiments. Signals were analyzed offline using Clampfit 9.0 software (Axon Instruments).

The voltage-clamp waveform protocols for each experiment are provided in the figures. The amplitude of I_{Ca} was calculated as the difference between peak inward current and the current at the end of the depolarizing pulse. I_{Ca} was normalized to the cell area by dividing the amplitude of I_{Ca} by the cell capacitance to give pA/pF. To assess the rate of inactivation of I_{Ca}, tau fast (τf) and tau slow (τs) inactivation components were derived by fitting a second-order exponential function to the decaying portion of I_{Ca} using the Chebyshev procedure (Clampfit software, Axon Instruments). Steady-state kinetic parameters were determined by fitting steady-state activation and inactivation data to Boltzmann equations to calculate the half-activating and half-inactivating potential (V_h) and the slope of activation and inactivation (k), as previously described (44). Recovery from inactivation of I_{Ca} was assessed by normalizing current amplitude at a constant test pulse (500 ms, −70 to 0 mV) to the constant prepulse value (500 ms, −70 to 0 mV) after various interpulse durations (50–350 ms, −70 mV, see Fig. 6). The contribution of I_{Ca} to total

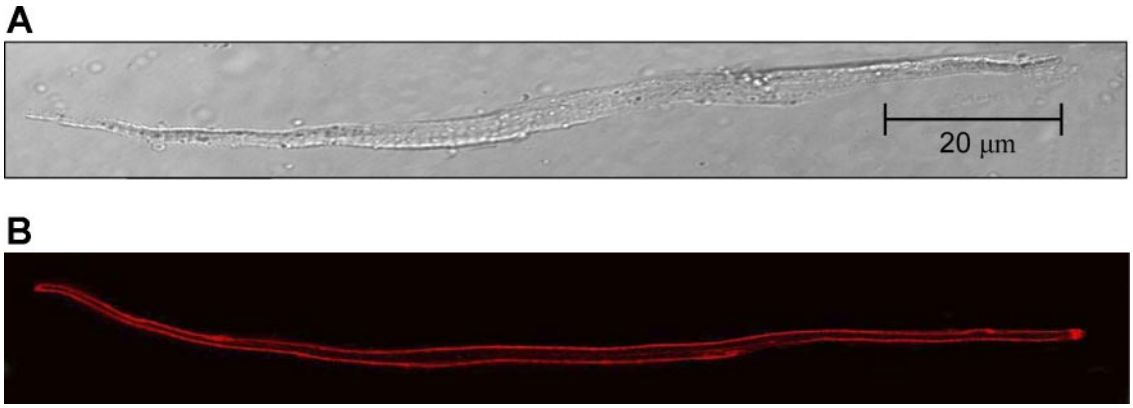

Fig. 1. Morphology of live ventricular myocytes from the turtle heart. *A*: light microscopy image. *B*: confocal microscopy image. Scale bar applies to both images. Mean morphometric data are provided in Table 1.

cellular [Ca^{2+}] was calculated from the transferred charges and cell volume. Charge transfer was determined by integrating the inactivating portion of the Ca^{2+} current for 500-ms square-wave voltage pulses from −70 mV to 0 mV. Cell volume was calculated from the measured cell capacitance (42.4 ± 1.9) and the surface-to-volume ratio of the cells. The myocytes were considered to be flat elliptical cylinders with an axis ratio of 1.2 for the elliptical cross section (34, 43, 44). The change in total cellular Ca^{2+} due to Ca^{2+} influx through L-type Ca^{2+} channels was expressed as a function of nonmitochondrial volume (34, 44).

Statistical Methods

With the exception of original traces and voltage protocols, data are given as mean values ± SE. *N* values are for number of cells in which the minimum number of animals is $n = 4$. Statistical tests are supplied in the appropriate figure legends.

RESULTS

Cell Morphology

Dissociation of the turtle heart required a higher concentration of digestive enzymes, longer perfusion times, and higher temperatures than those used previously for various fish species (32, 34, 43, 44). These differences may be due to variation in the structure of the extracellular matrix of the turtle heart compared with the fish heart or may relate to the complication of perfusing a three-chambered ventricle. Light and confocal microscopy images of isolated turtle ventricular myocytes are displayed in Fig. 1. Ventricular myocytes were typically spindle-shaped, being ~190 μm in length and 5–7 μm in width and depth (Table 1). When comparing the light and confocal images, it is apparent that the sarcomeres of the myocytes are not associated with T-tubules. Myocytes had a small cell volume (~2 pl), leading to a large surface area-to-volume ratio, typical of ectothermic vertebrates.

Turtle Ca^{2+} Transients and the Functional Significance of the SR

The functional significance of the SR was assessed via pharmacological blockade with ryanodine and thapsigargin (10 μM and 2 μM, respectively). Turtle myocytes were loaded with Fura 2 and field stimulated at 0.2 Hz in the absence and presence of SR blockade (Fig. 2). The amplitude of $[Ca^{2+}]_i$ was not significantly altered following inhibition of the SR (Fig. 2*B*), indicating the SR plays a small role in Ca^{2+} cycling on a beat-to-beat basis.

L-Type Ca^{2+} Channel Properties

Characterization of inward currents. A depolarizing voltage step from −80 mV to −40 mV elicited a fast-inactivating Na^+ current (I_{Na}) (Fig. 3*A*). As both I_{Na} and the L-type Ca^{2+} current (I_{Ca}) are activated within the same voltage range, we used TTX, a specific Na^+ channel blocker, to inhibit I_{Na} (Fig. 3*A*). Thus a voltage step from −80 mV to 0 mV in the presence of

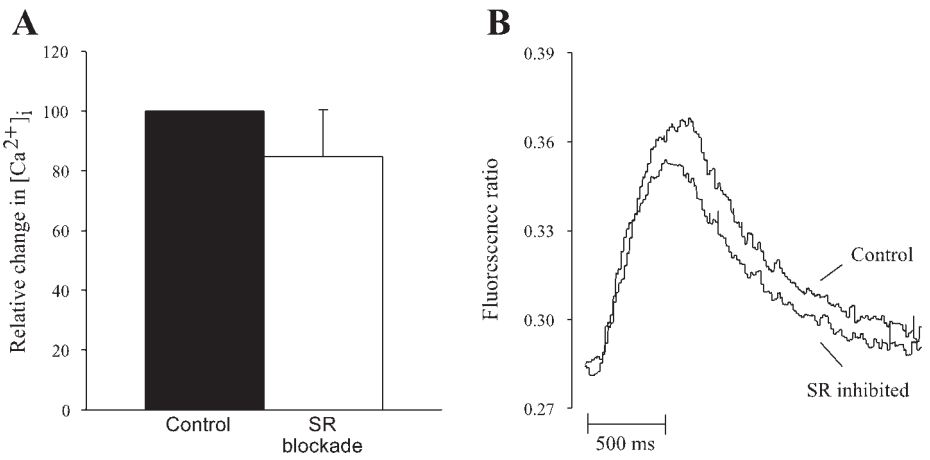

Fig. 2. The effect of inhibiting the sarcoplasmic reticulum (SR) on the turtle intracellular calcium transient $[Ca^{2+}]_i$. *A*: relative reduction in $[Ca^{2+}]_i$ due to SR inhibition with ryanodine (10 μM) and thapsigargin (2 μM). Values are means ± SE ($n = 6$). *B*: original traces of turtle $[Ca^{2+}]_i$ in the presence and absence of SR blockade. Statistical analysis (rank sum test) revealed no significant differences between control or SR-inhibited transients ($P > 0.05$).

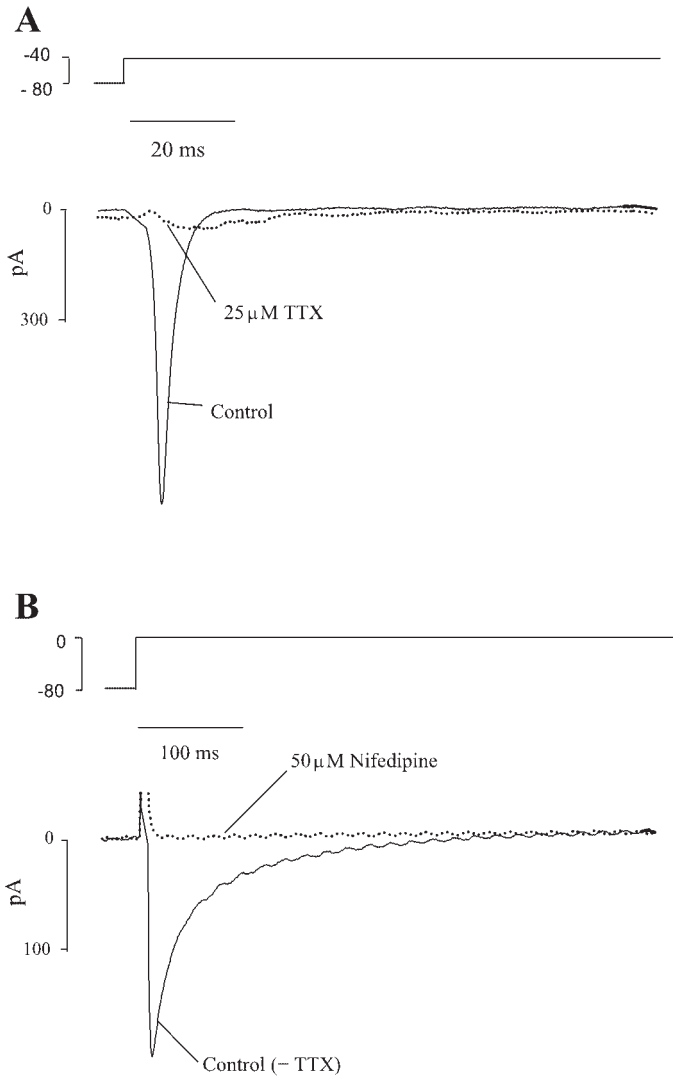

Fig. 3. Isolation of L-type Ca^{2+} current (I_{Ca}). *A*: effect of 25 μM TTX, a specific Na^+ channel blocker, on I_{Na} in a turtle ventricular myocyte (capacitance = 19.65 pF). *B*: effect of 50 μM nifedipine, a specific blocker of the L-type Ca^{2+} channel, on I_{Ca} in a turtle ventricular myocyte (capacitance = 44.9 pF) pretreated with 25 μM TTX. The waveform protocol used to activate I_{Ca} and I_{Na} is depicted above each current recording.

TTX gave rise to a slower activating and inactivating I_{Ca} (Fig. 3*B*). In previous studies on ectotherms, less than 1 μM TTX is sufficient to totally abolish I_{Na} (20, 32, 43). However, in turtle ventricular myocytes, we found much higher doses (25–40 μM) were necessary to abolish I_{Na} completely. Similar doses are used in mammalian preparations (6). Therefore, rather than blocking I_{Na} pharmacologically with high [TTX], prepulses from −70 mV to −40 mV were applied before each test pulse in all subsequent protocols to fully inactivate I_{Na} and experimentally isolate I_{Ca}. To be certain that the remaining current originated from L-type Ca^{2+} channels, we used 50 μM nifedipine, a specific L-type Ca^{2+} channel blocker, to inhibit I_{Ca} (Fig. 3*B*). A similar inhibition of I_{Ca} could be achieved with 100 μM $CdCl_2$ or 1 mM $NiCl_2$. The required dose of nifedipine is unusual for cardiac L-type Ca^{2+} channels (20, 32, 43) and may relate to the subunit composition of the L-type Ca^{2+} channel (see DISCUSSION).

In many species, I_{Ca} is known to deteriorate or "rundown" over time, particularly when measured in the whole-cell configuration. We assessed I_{Ca} rundown in turtle myocytes using the whole cell voltage-clamp technique (with various intracellular Ca^{2+} buffering) compared with the perforated-patch, voltage-clamp method (Fig. 4). Cells were depolarized from −70 mV to 0 mV, and I_{Ca} density was measured over a period of 12 min. In the whole cell configuration, I_{Ca} deteriorated to 50% of its original value within ~2 min, and to 20% after 12 min, regardless of the level of intracellular Ca^{2+} buffering (Fig. 4). In the perforated-patch configuration, I_{Ca} remained relatively stable and was only reduced by 10% over the entire 12-min period. Therefore, the perforated-patch, voltage-clamp technique was used in all subsequent experiments when measuring I_{Ca}. Interestingly, when using 5 mM EGTA or 5 mM BAPTA, the I_{Ca} density (3.8 ± 1.0 pA/pF and 4.2 ± 0.3 pA/pF, respectively) was similar to perforated-patch I_{Ca} density (3.2 ± 0.5 pA/pF). However, when using 25 μM EGTA, I_{Ca} density was considerably lower (1.54 ± 0.36 pA/pF). This suggests the buffering capacity of turtle myocytes is greater than 25 μM EGTA.

I_{Ca} density, kinetics and voltage relations. The current-voltage relationship for turtle ventricular myocytes is shown in Fig. 5. I_{Ca} activated at approximately −40 mV, peaked at 0 mV, and reversed at 60 mV. At peak I_{Ca} density (−3.2 ± 0.5 pA/pF), the time constant for fast inactivation (τf) and slow inactivation (τs) was 28.7 ± 1.5 ms and 169.2 ± 8.6 ms, respectively (n = 15). Because of this relatively slow inactivation time, charge transfer, and therefore total Ca^{2+} influx through L-type Ca^{2+} channels, was particularly high in turtle myocytes (Table 2).

Steady-state activation and inactivation of I_{Ca}. Activation of I_{Ca} began positive at −40 mV and was half maximal (V_h) at −3.9 ± 2.3 mV, while inactivation of I_{Ca}, or channel availability, began decreasing positive at −40 mV and was half complete at −22.5 ± 1.3 mV (Fig. 6). The slopes of activation

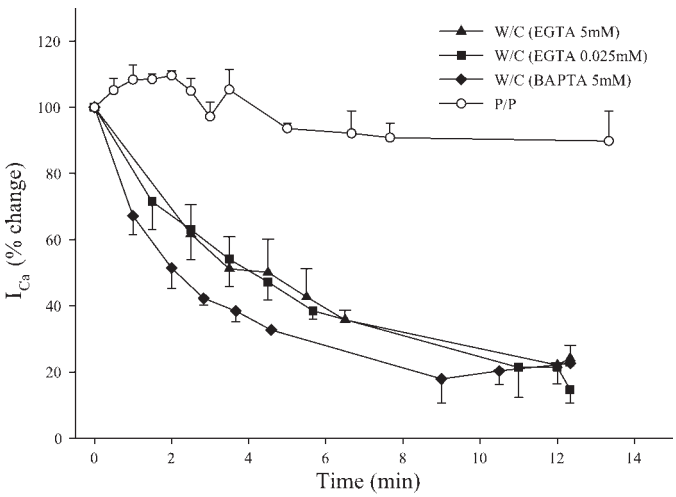

Fig. 4. Time-dependent change in amplitude of L-type Ca^{2+} current (I_{Ca}). Rundown of I_{Ca} was assessed using the whole cell voltage-clamp technique (W/C) at two different pipette concentrations of EGTA (0.025 mM, n = 4; 5 mM, n = 4), with BAPTA (5 mM, n = 5), and with the perforated-patch voltage-clamp technique (P/P) (n = 6). Because rundown of I_{Ca} was minimal in perforated-patch, this configuration of the voltage-clamp technique was used in all further experiments for assessment of I_{Ca}. Values are expressed as means ± SE.

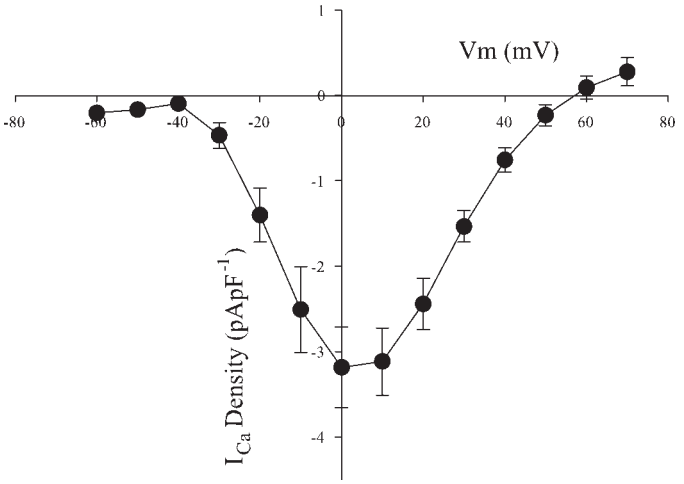

Fig. 5. L-type Ca^{2+} channel current-voltage relationships in turtle ventricular myocytes. I_{Ca} was normalized to myocyte capacitance (pF) and expressed as current density (pA pF^{-1}). Values are expressed as means ± SE (n = 15).

and inactivation (*k*) were 6.4 ± 0.7 and 4.4 ± 0.3, respectively. At voltages positive to 10 mV, channel inactivation was attenuated, probably due to a reduced driving force and consequently less Ca^{2+}-dependent inactivation. As a result of overlap between activation and inactivation curves, a window current was evident between −40 and 0 mV. The window current was maximal at approximately −18 mV, where it contributed 5% of maximal conductance (Fig. 6, *inset*).

I_{Ca} recovery from inactivation. The recovery of I_{Ca} from inactivation at −70 mV following 1-s prepulses to 0 mV is shown in Fig. 7. The number of recovered channels increased as the duration between the prepulse and the test pulse was lengthened. The time constant of recovery from inactivation (τ) was 157.3 ± 18.6 ms, thus at physiologically relevant frequencies of contraction (0.2–1 Hz), incomplete restitution of turtle L-type Ca^{2+} channels is unlikely to occur.

NCX Current Properties

Characterization of I_{NCX}. The capacity of the NCX to transfer charge is highly dependent on the intracellular $[Na^+]$. In mammalian cardiac myocytes, resting intracellular Na^+ concentration ($[Na^+]_i$) varies between species with a range of 4–15 mM (7) Because in vivo $[Na^+]_i$ is not known for turtle myocytes, we investigated the capacity of the NCX at a low (7 mM) and a high (14 mM) amount of Na^+ in the patch pipette. Membrane current was measured in the presence of 50 μM nifedipine to block I_{Ca}, and a combination of 10 μM ryanodine and 2 μM thapsigargin was used to inhibit possible SR Ca^{2+} release and reuptake. Under these conditions, a square-wave voltage pulse from −70 mV to 0 mV for 500 ms gave rise to a maintained outward current, which could be blocked with 10 mM $NiCl_2$, confirming the presence of a Ni^+-sensitive Na^+/Ca^{2+} exchange current (I_{NCX}). The Ni^{2+}-sensitive currents

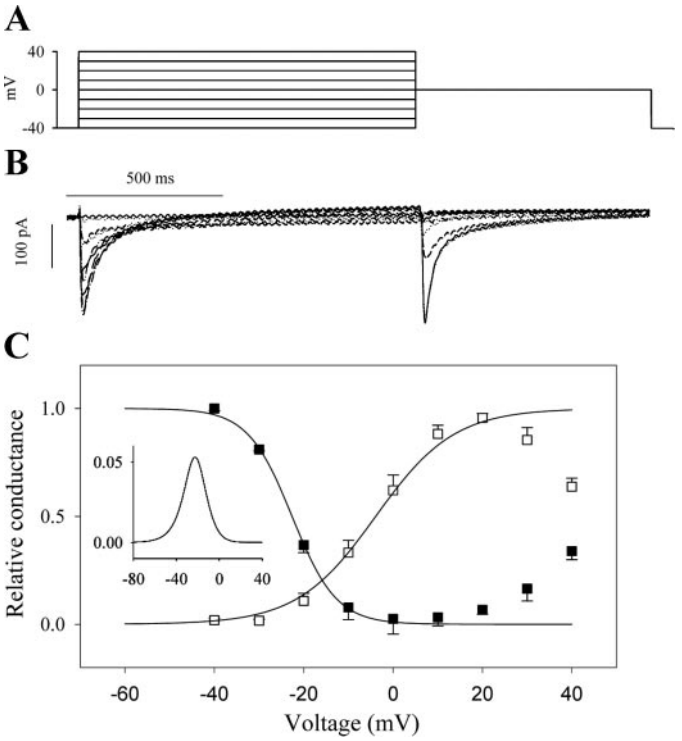

Fig. 6. Steady-state activation and inactivation of I_{Ca} in turtle ventricular cardiac myocytes. *A*: voltage protocol used to measure steady-state activation and inactivation. *B*: representative current recording from a turtle ventricular myocyte (capacitance = 78 pF) subjected to the voltage protocol given in *A*; *C*: mean steady-state inactivation and activation profiles. Values are means ± SE (*n* = 10). Inactivation (■) is measured by depolarizing from −70 mV to a test potential for 1 s and then testing the remaining available I_{Ca} at 0 mV. Activation (□) is calculated by dividing peak current by apparent driving force [applied membrane potential (Em) − reversal potential (Erev)] according to Ohm's law. *Inset*: L-type Ca^{2+} channel window current (product of activation and inactivation at each voltage).

elicited with 14 mM and 7 mM $[Na^+]_i$ are shown in Fig. 8. I_{NCX} was integrated to give a measure of charge transfer so that total Ca^{2+} influx through the NCX could be calculated. At 14 and 7 mM, intracellular Na^+, NCX charge transfer was 0.24 ± 0.1 and 0.12 ± 0.1, respectively, giving a total Ca^{2+} influx through the NCX at 0 mV of 58.5 ± 7.7 μmol/l and 26.7 ± 3.2 μmol/l, respectively (*n* = 9 and 7, Fig. 8). Total Ca^{2+} influx through the NCX was significantly greater with 14 mM than with 7 mM $[Na^+]_i$ (*P* = 0.004).

NCX voltage sensitivity. The voltage-dependence of the Na^+/Ca^{2+} exchange current was measured using a voltage ramp protocol in the presence of 50 μM nifedipine (Fig. 9, *inset*). I_{NCX} was identified as the Ni^{2+}-sensitive current. The measured reversal potential of I_{NCX} (ENCX) was ~30 mV, regardless of the intracellular Na^+ concentration (Fig. 9). The calculated ENCX under the present experimental conditions is 28.29 mV for 14 mM $[Na^+]_i$ and 80.68 mV for 7 mM $[Na^+]_i$. Thus, although the experimentally derived ENCX at 14 mM

Table 2. *Characterization of sarcolemmal Ca^{2+} influx through L-type channels in turtle ventricular myocytes*

Capacitance, pF	I_{Ca} Density, pA/pF	Charge Transfer, pC	Charge Density, pC/pF	Δ[Ca^{2+}]tot Non-M, μmol/l
42.4 ± 1.9	3.2±0.5	−11.3±1.7	−0.27±0.04	64.1±9.3

Data are expressed as means ± SE, *n* = 15. Δ[Ca^{2+}]tot Non-M, Change in total cellular [Ca^{2+}] expressed as a function of nonmitochondrial cell volume.

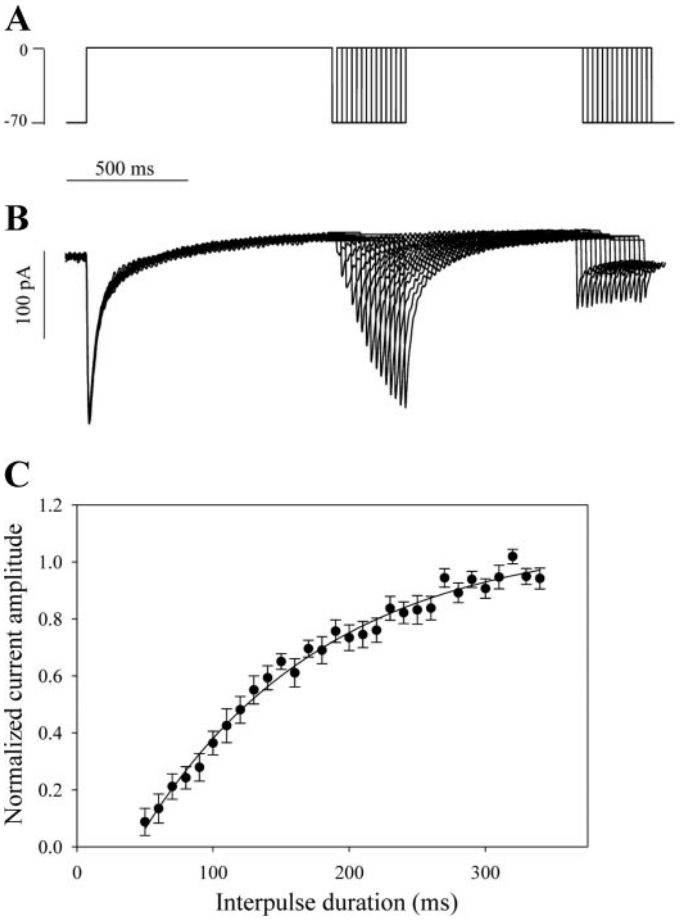

Fig. 7. Recovery of I_{Ca} from inactivation in turtle ventricular myocytes. *A*: voltage protocol used to measure recovery from inactivation. *B*: representative trace from a turtle ventricular myocyte (capacitance = 78.0) subjected to the displayed voltage protocol. *C*: relationship between current recovery and interpulse duration for ventricular myocytes. Values are expressed as means ± SE, $n = 10$.

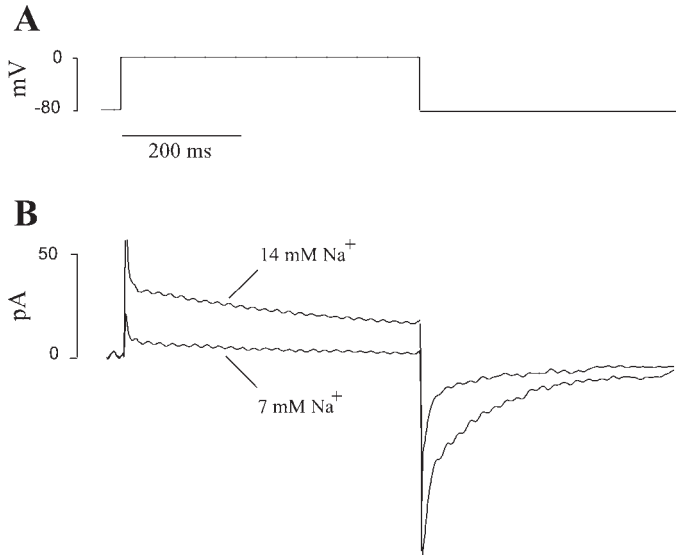

Fig. 8. Measurement of the Na^+/Ca^{2+} exchange current (I_{NCX}) using square wave voltage steps in turtle ventricular myocytes. *A*: voltage waveform protocol was applied in the absence and then the presence of $NiCl_2$ (10 mM), a blocker of the NCX. *B*: I_{NCX} was identified as the Ni^{2+}-sensitive current at each intracellular concentrations of Na^+: 14 and 7 mM.

$[Na^+]_i$ agrees well with the calculated value, it is expected that decreasing $[Na^+]_i$ will increase ENCX. A possible explanation for this discrepancy is that diastolic Ca^{2+} levels may also change when altering $[Na^+]_i$, which will also affect the measured ENCX.

At both 7 mM and 14 mM intracellular $[Na^+]$, the outward I_{NCX} current showed a steep increase with increasing voltage (outward rectification) (Fig. 9), while the inward current peaked at approximately −10 to −30 mV and then decreased at more negative voltages. I_{NCX} was significantly larger with 14 mM than with 7 mM $[Na^+]_i$ at almost all membrane voltages. Importantly, in the absence of the L-type Ca^{2+} channel and SR Ca^{2+} release, I_{NCX} was able to trigger contraction independently. This was the case with both concentrations of intracellular Na^+; however, at 14 mM $[Na^+]_i$, a greater degree of myocyte shortening occurred compared with 7 mM $[Na^+]_i$ (data not shown).

DISCUSSION

In the hearts of most ectothermic vertebrates, the SR seems to contribute little to contraction and relaxation (see Ref. 45). The cardiac muscle of many ectothermic species, including the turtle, are ryanodine insensitive and exhibit a postrest decay of force, suggesting SR independence, at least under normal physiological conditions (10, 12, 17, 41). In the present study, we tested SR involvement in cellular Ca^{2+} flux directly, and we show that inhibition of SR function with a combination of ryanodine and thapsigargin had little effect on $[Ca^{2+}]_i$ in turtle ventricular myocytes, supporting earlier findings on isolated muscle preparations (12). Thus, in the absence of a functional SR, the turtle heart will depend strongly on transsarcolemmal Ca^{2+} cycling for both the contraction and relaxation of the myocyte.

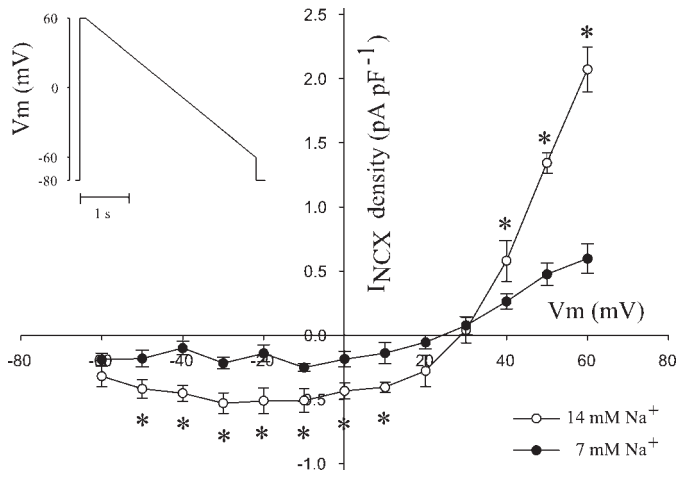

Fig. 9. Measurement of the I_{NCX} using ramp protocols (*inset*) in turtle ventricular myocytes. I_{NCX} was identified as the Ni^{2+}-sensitive current during the hyperpolarizing phase of the ramp pulse and was measured at two different intracellular concentrations of Na^+: 7 mM Na^+ ($n = 5$) and 14 mM Na^+ ($n = 5$). *Inset* shows voltage ramp protocol. Values are means ± SE. *Significant difference between data at 7 mM Na^+ and 14 mM Na^+ (one-way repeated-measures ANOVA; $P < 0.05$).

The importance of extracellular Ca^{2+} cycling in turtles, and the apparent lack of SR involvement has a clear ultrastructural basis. The morphological design of turtle myocytes reveals a system primed for transsarcolemmal Ca^{2+} flux. Turtle myocytes are spindle-shaped (long and thin) and lack T-tubules, which is typical of ectothermic vertebrates (45). The surface area-to-volume ratio (18.3) is high compared with mammalian ventricular myocytes (rabbit, 4.6; rat, 6–8) (2, 30), but similar to other ectotherms (trout, 18.2; crucian carp, 19.2; bluefin tuna, 14–17; mackerel, 18–22) (32, 42). This large surface area-to-volume ratio will enhance the efficacy of sarcolemmal Ca^{2+} transport by reducing the diffusional distance that Ca^{2+} has to travel to the myofilaments. Moreover, the myofilaments of ectothermic myocytes are subsarcolemmal (42), further promoting the close association of the sarcolemmal membrane and the contractile elements of the cell.

In most ectotherms, the majority of extracellular Ca^{2+} enters the cell through L-type Ca^{2+} channels (18, 34, 42). The central role of these channels can be demonstrated by an almost complete inhibition of force production by L-type Ca^{2+} channel blockers in fish (1). Our study demonstrates the turtle is no exception to this trend and relies strongly on this form of Ca^{2+} influx for contraction. The density and kinetics of turtle I_{Ca} are typical of other ectothermic species (20, 32, 42, 43). Steady-state activation and inactivation curves and the time taken for recovery from inactivation also coincide with those found in fish (32, 34, 42, 43). A sizeable window current exists at room temperature, which probably contributes to the prolongation of the action potential, and may be important in Ca^{2+} cycling at lower body temperatures (see Ref. 34).

Interestingly, although the density and kinetics of turtle I_{Ca}, with the exception of I_{Ca} time course of inactivation (see below), may be similar to other ectothermic species, the pharmacology suggests the turtle heart may predominantly contain L-type Ca^{2+} channels composed of a different subunit than most vertebrate cardiac L-type channels. The L-type Ca^{2+} channel is made up of a number of subunits, but the α_1-subunit is the main functional unit of the channel, responsible for pore formation and voltage sensitivity (35). In cardiac muscle, it exists as two main isoforms: α_{1C} and α_{1D} (8). The α_{1C} subunit is most commonly found in the mammalian myocardium and is characteristically sensitive to dihydropyridines (24). Conversely, the α_{1D} is found abundantly in neurons or pacemaker regions of the heart and requires a higher dose of dihydropyridines (~10–20-fold higher) to completely inhibit I_{Ca} (4, 22, 38, 46). Thus the pharmacology of the turtle L-type Ca^{2+} channel current may suggest the heart contains a large complement of α_{1D} subunits in their L-type Ca^{2+} channels. It is not clear what the functional significance of these channels may be in turtle ventricular myocytes; however, L-type Ca^{2+} channels containing the α_{1D} subunit have been linked with conduction of the action potential in the mammalian heart (23, 37, 47).

Our results indicate the turtle L-type Ca^{2+} channel is the predominant source of extracellular Ca^{2+}, with a total Ca^{2+} influx of 64.1 ± 9.3 of nonmitochondrial ($n = 15$) space. This value is 5 times that found in adult mammalian ventricular myocytes (5, 29) and approximately double that of certain fish ventricular cells (34, 42, 43). This difference is probably due to the relatively slow time course of inactivation of turtle I_{Ca} and may be a direct result of less Ca^{2+}-induced inactivation of the L-type Ca^{2+} channel and the lack of a functional SR. However, it must be noted that in similar experiments with fish, measurements were made in the whole cell configuration with intracellular buffering, which can increase the amplitude of I_{Ca} and therefore the rate of Ca^{2+}-dependent inactivation of the channel. Nevertheless, when compared with mammalian studies using a perforated-patch configuration, our results indicate the turtle L-type Ca^{2+} channel can contribute an enormous amount of Ca^{2+} for contraction, probably enough to support myocyte contraction independently of other cellular cycling mechanisms.

The large amount of Ca^{2+} that enters the cell during contraction via the L-type channels has to be removed to allow relaxation, and if the SR is not involved in the relaxation process, then another mechanism must be in place. In mammals, the SR and the NCX compete for the removal of Ca^{2+} during relaxation (6). Thus, in the absence of a functional SR, it is expected that the NCX will now act as the primary Ca^{2+} efflux pathway in turtle ventricular myocytes. In some species the NCX also contributes to contraction by entering "reverse mode" (Ca^{2+} in, Na^+ out) during the upsweep of the action potential. In the hearts of neonatal mammals, which are similar to turtle cardiac myocytes in both structure and function, the NCX accounts for 65–75% of total Ca^{2+} influx (27, 28), and among ectotherms, the NCX alone can activate contraction in the crucian carp or rainbow trout, with up to 50% of Ca^{2+} entry mediated through this reverse NCX activity (19, 44). Thus, in ectothermic vertebrates, and also mammalian neonates, the NCX may provide a substantial proportion of the activator Ca^{2+} necessary for contraction.

Measurement of NCX activity is complicated by the lack of information regarding the intracellular concentration of Na^+ in turtle ventricular myocytes. In fish, varying $[Na^+]_i$ greatly influences the activity of the NCX, with a reduction from 16 to 10 mM $[Na^+]_i$ leading to a 58% reduction in Ca^{2+} entry through the NCX (19). Thus we have measured the capacity of the NCX at two different concentrations of $[Na^+]_i$; 14 and 7 mM. Depolarizing voltage steps to 0 mV in the presence of L-type channel and SR blockade led to a nickel-sensitive outward current corresponding to a total Ca^{2+} influx of 58.5 ± 7.7 μmol/l ($n = 9$) and 26.7 ± 3.2 μmol/l ($n = 7$) at 14 and 7 mM $[Na^+]_i$, respectively. Importantly, at either concentration of $[Na^+]_i$, NCX Ca^{2+} entry was sufficient to support myocyte contraction independently. If we speculate that $[Na^+]_i$ in turtle ventricular myocytes is somewhere between 7 and 14 mM and we combine these figures with Ca^{2+} entry via L-type channels, we could expect a total Ca^{2+} influx at 0 mV via both mechanisms to amount to ~100 μmol/l. Of this, ~35% of activator Ca^{2+} originates from the NCX. This percentage is slightly higher than that seen in the crucian carp (~26%) when NCX activity was measured using similar voltage protocols and intracellular constituents. It is important to note that in the present study, L-type Ca^{2+} channels were inhibited with nifedipine, while measuring NCX activity. Previous studies measuring NCX activity in fish have suggested the presence of an intact Ca^{2+} current via L-type channels will increase forward mode NCX activity, due to the concentration-dependent nature of the exchanger and the reduced driving force for Ca^{2+} entry (19, 44). Thus our study may have overestimated the amount of Ca^{2+} entry via the NCX, although Hove-Madsen et al. (19) found that preserving I_{Ca} during depolarizing voltage steps had little effect on NCX Ca^{2+} entry at 0 mV. In any case, it seems

clear that the NCX is capable of contributing activator Ca^{2+} for contraction in turtle myocytes, and importantly, it is able to support myocyte contraction independent of the SR and L-type Ca^{2+} channels.

Perspectives

This is the first study to address cellular Ca^{2+} cycling in any reptilian species. Our results show that turtles, similar to most fish, rely predominantly on the L-type Ca^{2+} channel for delivering extracellular Ca^{2+} for contraction under routine environmental conditions. We also show that the NCX is a powerful route for both Ca^{2+} entry and Ca^{2+} removal. Freshwater turtles are renowned for their ability to tolerate a wide range of environmental challenges, and some species hibernate in aquatic habitats for up to 6 mo, subjecting themselves to large temperature fluctuations, long periods of hypoxia and anoxia, and consequential acidosis (15, 40). The mammalian myocardium is particularly sensitive to environmental change (6, 9, 11), which suggests the turtle heart may have physiological specializations in E-C coupling, which allow them to cope with their changing environment. The present study provides the groundwork for cellular studies on ion regulation of contractility in reptilian cardiomyocytes. Thus future studies should be aimed at investigating how these Ca^{2+} flux pathways are affected by temperature, hypoxia, and acidosis to provide mechanistic insight into the stress tolerance of the turtle heart.

ACKNOWLEDGMENTS

We especially thank Prof. David Eisner and Dr Andrew Trafford for their helpful advice and technical expertise.

GRANTS

This study was funded by The BBSRC, The Welcome Trust, The Company of Biologists, and The Anglo-Danish Society.

REFERENCES

1. **Aho E and Vornanen M.** Comparison of contractile properties of atrial and ventricular tissue of the rainbow trout (*Oncorhynchus mykiss*) heart: effects of thermal acclimation. *J Exp Biol* 202: 2663–2677, 1999.
2. **Barth E, Stammler G, Speiser B, and Schaper J.** Ultrastructural quantification of mitochondria and myofilaments in cardiac muscle from 10 different animal species including man. *J Mol Cell Cardiol* 24: 669–681, 1992.
3. **Bassani JW, Bassani RA, and Bers DM.** Relaxation in rabbit and rat cardiac cells: species-dependent differences in cellular mechanisms. *J Physiol* 476: 279–293, 1994.
4. **Bell DC, Butcher AJ, Berrow NS, Page KM, Brust PF, Nesterova A, Stauderman KA, Seabrook GR, Nurnberg B, and Dolphin AC.** Biophysical properties, pharmacology, and modulation of human, neuronal L-type (alpha(1D), Ca(V)1.3) voltage-dependent calcium currents. *J Neurophysiol* 85: 816–827, 2001.
5. **Berlin JR, Bassani JW, and Bers DM.** Intrinsic cytosolic calcium buffering properties of single rat cardiac myocytes. *Biophys J* 67: 1775–1787, 1994.
6. **Bers DM.** *Excitation Contraction Coupling and Cardiac Contractile Force.* London: Kluwer Academic, 2001.
7. **Bers DM, Barry WH, and Despa S.** Intracellular Na^+ regulation in cardiac myocytes. *Cardiovasc Res* 57: 897–912, 2003.
8. **Doering CJ and Zamponi GW.** Molecular pharmacology of high voltage-activated calcium channels. *J Bioenerg Biomembr* 35: 491–505, 2003.
9. **Donaldson SKB and Hermansen L.** Differential, direct effects of H^+ on Ca^{2+} activated force of skinned fibers from the soleus, cardiac and adductor magnus muscles of the rabbit. *Pflügers Arch* 376: 55–65, 1978.
10. **Driedzic WR and Gesser H.** Differences in force-frequency relationships and Ca^{2+} dependency between elasmobranches and teleost hearts. *J Exp Biol* 140: 227–241, 1988.
11. **Fabiato A and Fabiato F.** Effects of pH on the myofilaments and the sarcoplasmic reticulum of skinned cells from cardiac and skeletal muscles. *J Physiol* 276: 233–255, 1978.
12. **Galli GLJ, Gesser H, Taylor EW, Shiels HA, and Wang T.** The role of the sarcoplasmic reticulum in the generation of high heart rates and blood pressures in reptiles. *J Exp Biol* 209: 1956–1963, 2006.
13. **Gesser H.** Cardiac force-interval relationship, adrenaline and sarcoplasmic reticulum in rainbow trout. *J Comp Physiol* 166B: 278–285, 1996.
14. **Haddock PS, Coetzee WA, Cho E, Porter L, Katoh H, Bers DM, Jafri MS, and Artman M.** Subcellular $[Ca^{2+}]_i$ gradients during excitation-contraction coupling in newborn rabbit ventricular myocytes. *Circ Res* 85: 415–427, 1999.
15. **Herbert CV and Jackson DC.** Temperature effects on the responses to prolonged submergence in the turtle *Chrysemys picta bellii.* II. Metabolic rate, blood acid-base and ionic changes, and cardiovascular function in aerated and anoxic water. *Physiol Zool* 58: 670–681, 1985.
16. **Hove-Madsen L.** The influence of temperature on ryanodine sensitivity and the force-frequency relationship in the myocardium of rainbow trout. *J Exp Biol* 167: 47–60, 1992.
17. **Hove-Madsen L and Gesser H.** Force frequency relation in the myocardium of rainbow trout. Effects of K^+ and adrenaline. *J Comp Physiol B* 159: 61–69, 1989.
18. **Hove-Madsen L, Llach A, Tibbits GF, and Tort L.** Triggering of sarcoplasmic reticulum Ca^{2+} release and contraction by reverse mode Na^+/Ca^{2+} exchange in trout atrial myocytes. *Am J Physiol Regul Integr Comp Physiol* 284: R1330–R1339, 2003.
19. **Hove-Madsen L, Llach A, and Tort L.** Na^+/Ca^{2+}-exchange activity regulates contraction and SR Ca^{2+} content in rainbow trout atrial myocytes. *Am J Physiol Regul Integr Comp Physiol* 279: R1856–R1864, 2000.
20. **Hove-Madsen L and Tort L.** L-type Ca^{2+} current and excitation-contraction coupling in single atrial myocytes from rainbow trout. *Am J Physiol Regul Integr Comp Physiol* 275: R2061–R2069, 1998.
21. **Keen JE, Vianzon DM, Farrell AP, and Tibbits GF.** Effect of temperature and temperature acclimation on the ryanodine sensitivity of the trout myocardium. *J Comp Biochem Physiol A* 124: 369–382, 1994.
22. **Koschak A, Reimer D, Huber I, Grabner M, Glossmann H, Engel J, and Striessnig J.** Alpha 1D (Cav1.3) subunits can form L-type Ca^{2+} channels activating at negative voltages. *J Biol Chem* 276: 22100–22106, 2001.
23. **Mangoni ME, Couette B, Bourinet E, Platzer J, Reimer D, Striessnig J, and Nargeot J.** Functional role of L-type Cav1.3 Ca^{2+} channels in cardiac pacemaker activity. *Proc Natl Acad Sci USA* 100: 5543–5548, 2003.
24. **Mikami A, Imoto K, Tanabe T, Niidome T, Mori Y, Takeshima H, Narumiya S, and Numa S.** Primary structure and functional expression of the cardiac dihydropyridine-sensitive calcium channel. *Nature* 340: 230–233, 1989.
25. **Minajeva A, Kaasik A, Paju K, Seppet E, Lompre AM, Veksler V, and Ventura-Clapier R.** Sarcoplasmic reticulum function in determining atrioventricular contractile differences in rat heart. *Am J Physiol Heart Circ Physiol* 273: H2498–H2507, 1997.
26. **Morad M, Goldman YE, and Trentham DR.** Rapid photochemical inactivation of Ca^{2+}-antagonists shows that Ca^{2+} entry directly activates contraction in frog heart. *Nature* 304: 635–638, 1983.
27. **Nakanishi T, Okuda H, Kamata K, Abe K, Sekiguchi M, and Takao A.** Development of myocardial contractile system in the fetal rabbit. *Pediatr Res* 22: 201–207, 1988.
28. **Nassar R, Reedy MC, and Anderson PA.** Developmental changes in the ultrastructure and sarcomere shortening of the isolated rabbit ventricular myocyte. *Circ Res* 61: 465–483, 1987.
29. **Negretti N, Varro A, and Eisner DA.** Estimate of net calcium fluxes and sarcoplasmic reticulum calcium content during systole in rat ventricular myocytes. *J Physiol* 486: 581–591, 1995.
30. **Satoh H, Delbridge LM, Blatter LA, and Bers DM.** Surface:volume relationship in cardiac myocytes studied with confocal microscopy and membrane capacitance measurements: species-dependence and developmental effects. *Biophys J* 70: 1494–1504, 1996.
31. **Shiels HA and Farrell AP.** The effects of temperature and adrenaline on the relative importance of the sarcoplasmic reticulum in contributing Ca^{2+} to force development in isolated ventricular trabeculae from rainbow trout. *J Exp Biol* 200: 1607–1621, 1997.
32. **Shiels HA, Blank JM, Farrell AP, and Block BA.** Electrophysiological properties of the L-type Ca^{2+} current in cardiomyocytes from bluefin tuna

and Pacific mackerel. *Am J Physiol Regul Integr Comp Physiol* 286: R659–R668, 2004.
33. **Shiels HA, Freund EV, Farrell AP, and Block BA.** The sarcoplasmic reticulum plays a major role in isometric contraction in atrial muscle of yellowfin tuna. *J Exp Biol* 202: 881–990, 1999.
34. **Shiels HA, Vornanen M, and Farrell AP.** Temperature dependence of L-type Ca^{2+} channel current in atrial myocytes from rainbow trout. *J Exp Biol* 203: 2771–2880, 2000.
35. **Sieber M, Nastainczyk W, Zubor V, Wernet W, and Hofmann F.** The 165-kDa peptide of the purified skeletal muscle dihydropyridine receptor contains the known regulatory sites of the calcium channel. *Eur J Biochem* 167: 117–122, 1987.
36. **Sutko JL and Willerson JT.** Ryanodine alteration of the contractile state of rat ventricular myocardium. Comparison with dog, cat, and rabbit ventricular tissues. *Circ Res* 46: 332–343, 1980.
37. **Takemura H, Yasui K, Opthof T, Niwa N, Horiba M, Shimizu A, Lee JK, Honjo H, Kamiya K, Ueda Y, and Kodama I.** Subtype switching of L-Type Ca^{2+} channel from Cav1.3 to Cav12 in embryonic murine ventricle. *Circ J* 69: 1405–1411, 2005.
38. **Takimoto K, Li D, Nerbonne JM, and Levitan ES.** Distribution, splicing and glucocorticoid-induced expression of cardiac alpha 1C and alpha 1D voltage-gated Ca^{2+} channel mRNAs. *J Mol Cell Cardiol* 29: 3035–3042, 1997.
39. **Tibbits G, Hove-Madsen L, and Bers DM.** Calcium transport and the regulation of cardiac contractility in teleosts—a comparison with higher vertebrates. *Can J Zool* 69: 2014–2019, 1991.
40. **Ultsch GR and Jackson DC.** Long-term submergence at 3 degrees C of the turtle *Chrysemys picta bellii* in normoxic and severely hypoxic water. III Effects of changes in ambient Po_2 and subsequent air breathing. *J Exp Biol* 97: 87–99, 1982.
41. **Vornanen M.** Regulation of contractility of the fish (*Carassius carassius*) heart ventricle. *Comp Biochem Physiol* 94C: 477–483, 1989.
42. **Vornanen M.** Sarcolemmal Ca influx through L-type Ca channels in ventricular myocytes of a teleost fish. *Am J Physiol Regul Integr Comp Physiol* 272: R1432–R1440, 1997.
43. **Vornanen M.** L-type Ca^{2+} current in fish cardiac myocytes: effects of thermal acclimation and â-adrenergic stimulation. *J Exp Biol* 201: 533–547, 1998.
44. **Vornanen M.** Na^{+}-Ca^{2+} exchange current in ventricular myocytes of fish heart: contribution to sarcolemmal Ca^{2+} influx. *J Exp Biol* 202: 1763–1775, 1999.
45. **Vornanen M, Shiels HA, and Farrell AP.** Plasticity of excitation-contraction coupling in fish cardiac myocytes. *Comp Biochem Physiol A* 132: 827–846, 2002.
46. **Xu W and Lipscombe DJ.** Neuronal Ca(V)1.3alpha(1)L-type channels activate at relatively hyperpolarized membrane potentials and are incompletely inhibited by dihydropyridines. *Neuroscience* 21: 5944–5951, 2001.
47. **Zhang Z, Xu Y, Song H, Rodriguez J, Tuteja D, Namkung Y, Shin HS, and Chiamvimonvat N.** Functional roles of Ca(v)1.3 (alpha(1D)) calcium channel in sinoatrial nodes: insight gained using gene-targeted null mutant mice. *Circ Res* 90: 981–987, 2002.